Mechanical properties and decomposition performance of peelable coating containing UiO-66 catalyst and waterborne silane-terminated polyurethane dispersions

Kyung-Min Kim, Hee-Woong Park, Gyu-Seong Shim, Seong-Wook Jang, Hyun-Joong Kim, Gyeong-Seok Chae, Seunghan Shin & Jung-Hyun Lee

Journal of Materials Science

ISSN 0022-2461
Volume 55
Number 6

J Mater Sci (2020) 55:2604-2617
DOI 10.1007/s10853-019-04184-2

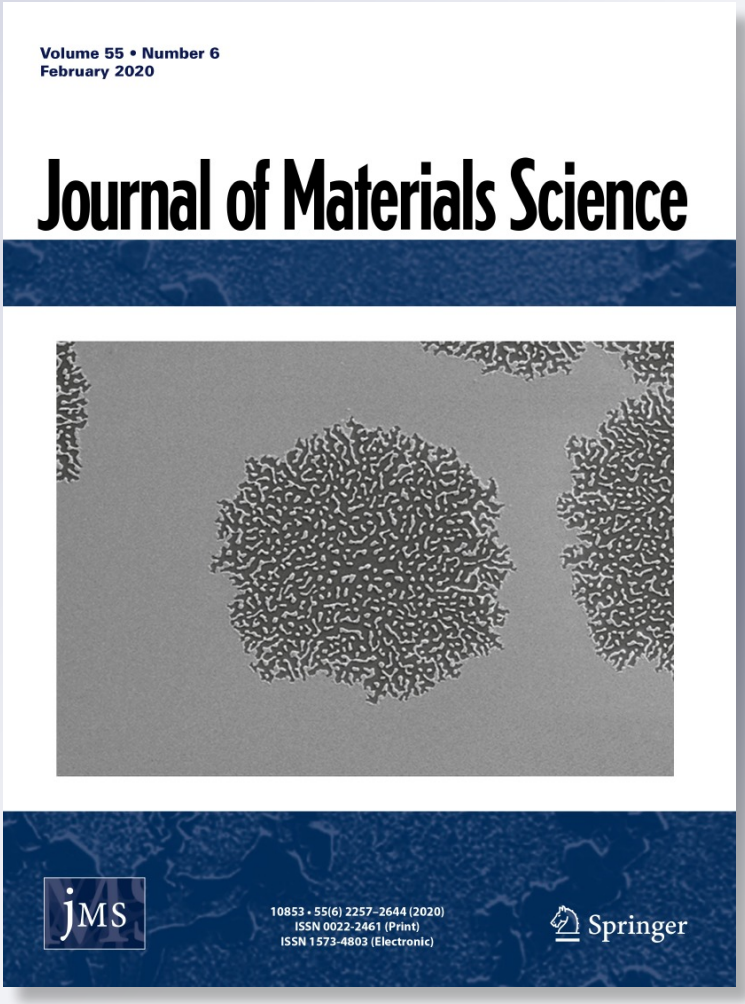

Springer

J Mater Sci (2020) 55:2604–2617

Polymers & biopolymers

Mechanical properties and decomposition performance of peelable coating containing UiO-66 catalyst and waterborne silane-terminated polyurethane dispersions

Kyung-Min Kim[1], Hee-Woong Park[2,4], Gyu-Seong Shim[1], Seong-Wook Jang[1], Hyun-Joong Kim[1,*], Gyeong-Seok Chae[2,3], Seunghan Shin[2,3,*], and Jung-Hyun Lee[4]

[1] *Laboratory of Adhesion and Bio-Composites, Program in Environmental Materials Science, Research Institute of Agriculture and Life Sciences, College of Agriculture and Life Sciences, Seoul National University, Seoul 08826, Republic of Korea*

[2] *Green Chemistry and Materials Group, Korea Institute of Industrial Technology (KITECH), Cheonan 31056, Republic of Korea*

[3] *Department of Green Process and System Engineering, Korea University of Science and Technology (UST), Cheonan 31056, Republic of Korea*

[4] *Department of Chemical and Biological Engineering, Korea University, Seoul 02841, Republic of Korea*

Published online:
13 November 2019

ABSTRACT

An easily peelable coating was prepared using silane-terminated polyurethane dispersions (SPUDs) and UiO-66 catalyst (a zirconium(IV)-based metal–organic framework), to capture and decompose the nerve agent simulant, methyl paraoxon (MPO), at room temperature. SPUDs were used as the binder. The peel strength of the SPUD film containing UiO-66 decreased with increasing UiO-66 content, and the film with 40 wt% UiO-66 could not be easily peeled off. In contrast, the SPUD/PVB/UiO-66 peelable coating film could be easily peeled off. With increasing UiO-66 content, the Young's moduli of the SPUD/UiO-66 and SPUD/PVB/UiO-66 coating films gradually increased, while the elongation decreased. The increase in the glass transition temperature was less than approximately 5%, depending on the UiO-66 content of the SPUD/UiO-66 film. Two peaks of tan δ appeared for the SPUD/PVB/UiO-66 coating film. As the UiO-66 content increased, the second peak shifted to the right. This could be attributed to the bond strength between the mixed polymeric binder and the nanoparticles. Furthermore, MPO decomposition by the SPUD/PVB/UiO-66 coating film increased with increasing UiO-66 content. These findings suggest the possibility of the development of a peelable coating film for the capture and decomposition of MPO.

Address correspondence to E-mail: hjokim@snu.ac.kr; shshin@kitech.re.kr

https://doi.org/10.1007/s10853-019-04184-2

Abbreviations

GPC	Gel permeation chromatography
Tg	Glass transition temperature
MOF	Metal–organic framework
MPO	Methyl paraoxon
PVB	Poly(vinyl butyral)
SPUD	Silane-terminated polyurethane dispersion

Introduction

Metal–organic frameworks (MOFs) have a porous crystalline structure and inherent properties of hybrid solids such as low density and high surface area. MOFs are used in a variety of applications such as sensing [1], catalysis [2, 3], gas separation [4], gas storage [5], drug delivery [6], and the removal of toxic substances [7]. In particular, UiO-66 is composed of twelve 1,4-benzenedicarboxylic acid linkers coordinated to the metal atoms of $Zr_6O_4(OH)_4$ octahedra, resulting in a highly packed face-centered cubic structure [8].

Recently, nanosized MOF particles have been studied [9–12]. The nanostructures of porous MOFs provide higher efficiency because of a larger external surface area. In particular, the studies on the decomposition of organic phosphates, which are used as nerve agent simulant, by UiO-66 are crucial for industrial and military researches. The coating of such a catalyst with a nanosized MOF that dispersed in a polymer coating has a wide range of application. Recently, zirconium-based MOFs have been extensively studied owing to their high thermal, mechanical, and hydrolytic stabilities. Extensive research has been conducted to determine the thermal, mechanical, and viscoelastic properties of peelable coatings containing MOF particles. Alternatively, the decomposition of methyl paraoxon (MPO) using a polyurethane coating, in which MOF-structured UiO-66 was dispersed, has been evaluated in some of the studies.

To use the UiO-66 catalyst in polymer coating films, the selection of the binder is important. For military and industrial applications, the polymer coating films may be applied as a peelable coating on a substrate, dried, and then peeled easily. Peelable coatings as temporary protective coatings are mainly used to protect surfaces during the manufacture, assembly, and transportation of products and components. These coatings are used to prevent surface damage and to simplify the cleaning operation. Peelable coatings that are removable after drying can be prepared using rubber-based paints, poly(vinyl alcohol) (PVA) resin, poly(vinyl acetate) resin, poly(vinyl butyral) (PVB) resin, and waterborne polyurethane dispersions (WPUDs) [13–16]. WPUDs are environmentally friendly and are used in many applications such as coatings, adhesives, and finishes. When WPUD is used in the temporary protective coating of a product, it can be peeled easily after drying. Peelability is a very important factor for peelable coatings. WPUD coatings generally have a high peel strength because of low cohesion due to the lack of cross-linking. The film properties and adhesive properties of WPUDs are mainly determined by the polyol and polymer chain structures [17, 18]. Self-cross-linking has been induced by introducing a silanol group to improve the physical properties of WPUD. A few papers have reported on silane-terminated polyurethane dispersions (SPUDs) prepared by the acetone process [19]. Recently, studies on SPUD synthesis without the use of an organic solvent have been actively conducted [20].

SPUDs are synthesized by the acetone process, in which waterborne PU is synthesized and dispersed in water to obtain waterborne SPUDs. The PU prepolymer terminated with the NCO group contains carboxylate in the backbone. The terminal NCO group of the PU prepolymer is reacted with (3-aminopropyl)triethoxysilane (APTES) to obtain a SPU capped with a silane group. Finally, waterborne SPUDs were obtained by dispersing in water. The characteristics of the SPUDs were determined by gel permeation chromatography (GPC), Fourier transform infrared (FTIR) spectroscopy, and particle size analysis of the synthesized SPUD binder.

This is a fundamental study on the application of a peelable coating to military equipment for preventing secondary pollution by capturing and decomposing pollutants and chemical agents. In this study, a UiO-66 catalyst with a nanoporous MOF structure was dispersed in SPUDs to fabricate a peelable coating. The polymer coating film was prepared by varying the UiO-66 content. The peel strength of the coating containing the functional catalyst for easy removal after drying was determined, and the tensile properties and viscoelastic behavior were studied. In addition, the performance of the UiO-66 catalyst in

the polymer coating film in the decomposition of MPO was investigated.

Materials and methods

Materials

The following chemicals were used in the study: 2,2-bis(hydroxymethyl)propionic acid (DMPA, Sigma-Aldrich, USA), isophorone diisocyanate (IPDI, Sigma-Aldrich, USA), poly(tetrahydrofuran) (PTMG, M_n = ~ 1000 g/mol, Sigma-Aldrich, USA), acetone (Sigma-Aldrich, USA), ethylene glycol (EG, 99.8%, Sigma-Aldrich, USA), (3-aminopropyl)triethoxysilane (APTES, Sigma-Aldrich, USA), triethylamine (TEA, Sigma-Aldrich, USA), PVB (Sigma-Aldrich, USA), ethyl alcohol (EtOH, 99.5%, Samchun, Republic of Korea), 1-methyl-2-pyrrolidone (NMP, Sigma-Aldrich, USA), and dibutyltin dilaurate (DBTDL, 95%, Sigma-Aldrich, USA).

Terephthalic acid (98%, Sigma-Aldrich, USA), zirconium(IV) chloride ($ZrCl_4$, ≥ 99.5%, Sigma-Aldrich, USA), *N*,*N*-dimethylformamide (DMF, ≥ 99.8%, Sigma-Aldrich, USA), hydrochloric acid (HCl, Sigma-Aldrich, USA), and EtOH (99.5%, Sigma-Aldrich, USA) were used for the synthesis of UiO-66. 4-Ethylmorpholine (4-EM, > 99.0%, TCI, Japan), MPO (Sigma-Aldrich, USA), and methanol (anhydrous, 99.8%, Sigma-Aldrich, USA) were used in the hydrolysis experiments.

Synthesis and characterization of waterborne SPUDs and UiO-66 (Zr(IV)-based MOF) catalyst

SPUDs were synthesized using the acetone method (Scheme 1). The DMPA-based WPUD affects the hard segment content of the synthesized WPUD and the mechanical properties of the peelable coating, depending on the molecular weight of poly(tetrahydrofuran) (PTMG) [21]. If the tensile strength is too high, the film will break; if the elongation is too high, the peelable coating film would peel off. Therefore, polyol was selected as PTMG to achieve intermediate values in both tensile strength and elongation for the peelable coating film. In addition, the silane group was introduced to increase the cross-linking density and hence increase the tensile strength. DMPA (12 g, 0.089 mol), NMP (15 g), and PTMG (164.56 g, ~ 0.165 mol) were charged into a 2-L double-jacketed glass reactor and stirred at 75 °C at 300 rpm for 15 min under argon atmosphere. IPDI (84.18 g, 0.379 mol) and DBTDL (catalyst, 0.16 wt% of the total solids (0.46 g)) were mixed and dropped over 5 min into the glass reactor, and the mixture was stirred at 300 rpm for 3 h. Then, EG (6.24 g, 0.101 mol) was slowly dropped and stirred at 300 rpm for 2 h. The reaction mixture was cooled to 40 °C, and 200 mL of acetone was added. Then, TEA (9.05 g, 0.089 mol) was dropped and stirred for 1 h. APTES (11.13 g, 0.050 mol) was slowly dropped, and the mixture was stirred at 300 rpm for 1 h. After lowering the temperature to room temperature, distilled water (432.53 g) was added to the mixture under stirring at 800 rpm so that the final solid content was approximately 38% (theoretically 40%). The mixture was then stirred at 1000 rpm for 1 h to disperse water. Rotary evaporation was performed at room temperature for 30 min to 1 h to remove the solvent.

UiO-66 was synthesized as follows: Terephthalic acid (0.86 mol, 142 g) and $ZrCl_4$ (0.86 mol, 200 g) were added to 6266 mL of DMF (86 mol, 100 eq) in a 10-L glass bottle and stirred using a magnetic bar at room temperature for 2 h to dissolve the compounds. A 37 wt% HCl solution (0.86 mol, 95 g) was added, and the reaction was allowed to proceed in a 120 °C conventional oven for 24 h to dissolve the compounds. After diluting with DMF, the mixture was filtered, and a white precipitate was collected. The solid was washed with excess DMF and ethanol three times for 24 h each. Finally, the obtained UiO-66 was dried at 80 °C for 12 h (total yield: ~ 60%).

The number average molecular weight (M_n) and the polydispersity (M_w/M_n) were determined by GPC (PL-GPC 220, Agilent Technologies, USA) performed at 25 °C using THF as the eluent at a flow rate of 1 mL min^{-1} using polystyrene calibration standards. FTIR spectroscopy was performed in the transmittance mode (NICOLET 6700, Thermo Electron Co., USA) in the range of 600–4000 cm^{-1} with a resolution of 4 cm^{-1}. The specimens were measured after forming KBR pellets. The particle size was measured using a particle size analyzer (ELS-Z2, Otsuka Electronics Co., Japan) at 25 °C in distilled water. The measurements were repeated three times, and the average size was recorded.

The structure of the synthesized UiO-66 was determined by field-emission scanning electron microscopy (FESEM SUPRA 55VP, Carl Zeiss,

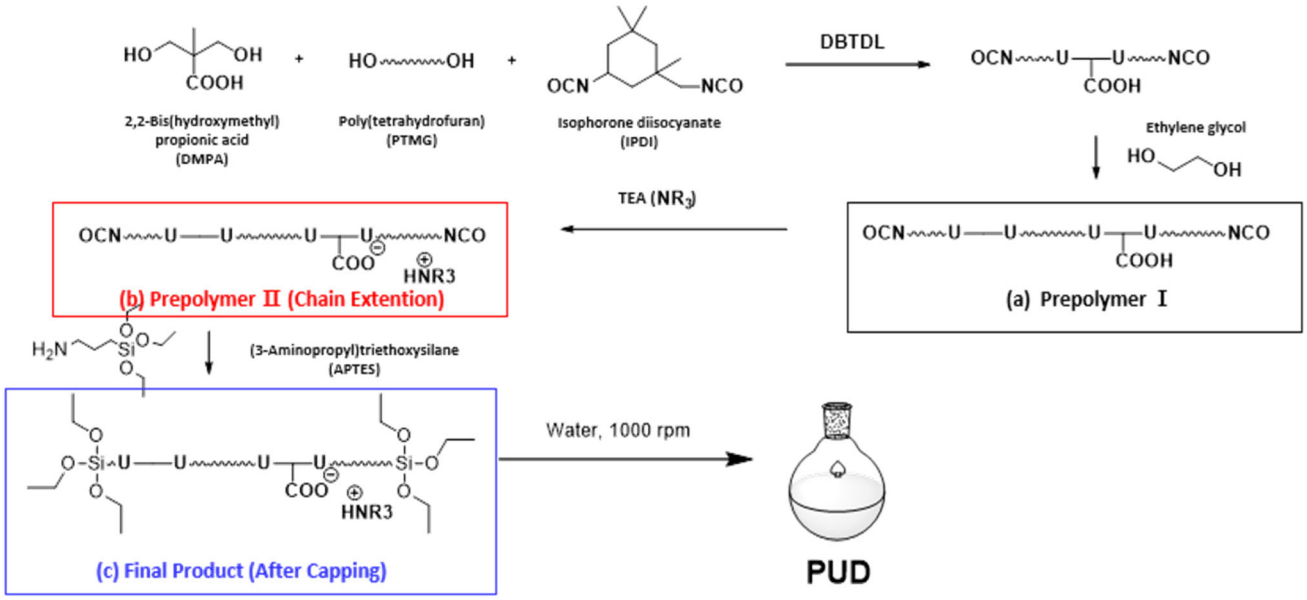

Scheme 1 Synthesis of waterborne silane-terminated polyurethane dispersions (SPUD).

Germany). The crystalline phase of the synthesized powders was analyzed by powder X-ray diffraction (PXRD) spectroscopy (D8 Advance, Bruker, USA) performed at 45 kV and 100 mA using CuKα radiation with λ = 0.15406 nm in the 2θ angle range of 5°–40° with a step size of 0.02° at a scanning rate of 2° min^{-1}. The specific surface area, total pore volume, and average pore size were measured using a Brunauer–Emmett–Teller (BET) instrument (ASAP-2010, Micromeritics Instrument Corporation, USA). All the samples were analyzed by the BET method after pretreatment at 200 °C for 6 h in vacuum.

Preparation of the peelable coating material

First, UiO-66 was dispersed in EtOH at a solid content of 10% using a paste mixer (ARV-310, Thinky, Japan) at 2000 rpm for 10 min. Then, PVB was dissolved in EtOH at a solid content of 20% using the paste mixer at 2000 rpm for 30 min. Subsequently, the dispersed UiO-66 nanoparticles were added in stages to the SPUD solution corresponding to the wt% equation below [Eqs. (1) and (2)].

$$\text{UiO-66 (wt\%)} = \left(\frac{W_{UiO66}}{W_{UiO66} + W_{Binder}}\right) \times 100\%, \quad (1)$$

where

$$W_{Binder} = W_{PVB} + W_{SPUDs}. \quad (2)$$

Here, W_{UiO66} is the weight of UiO-66 nanoparticles dispersed in EtOH, W_{PVB} is the weight of PVB in the PVB solution, and W_{SPUDs} is the weight of SPU in the SPUDs. Five coating films were prepared by varying the UiO-66 content (10, 20, 30, 40, and 60 wt% with respect to the binder content as Table 1).

Two types of binders were used: (a) SPUD and (b) SPUD/PVB (70:30). In the case of mixed binder, the SPUD and PVB solutions were mixed using the paste mixer at 2000 rpm for 10 min. Then, the mixture was allowed to stand for 30 min. Finally, UiO-66, SPUD and PVB mixture, and EtOH were blended

Table 1 Formulation of SPUD/UiO-66 and SPUD/PVB/UiO-66 peelable coating

Sample	SPUD (wt%)	PVB (wt%)	UiO-66 (wt%)
Neat	100		
UiO 10	90		10
UiO 20	80		20
UiO 30	70		30
UiO 40	60		40
UiO 60	40		60
D70/P30/UiO 10	70	30	0
D70/P30/UiO 10	63	27	10
D70/P30/UiO 20	56	24	20
D70/P30/UiO 30	49	21	30
D70/P30/UiO 40	42	18	40
D70/P30/UiO 60	28	12	60

using the paste mixer at 2000 rpm for 3 min. The solid content of the mixture was approximately 10%.

Fabrication of peelable coating

In order to replicate the actual application of the peelable coating (i.e., as the outmost layer on the painted steel of a military tank), we applied a matte enamel paint (thickness: 50 μm, Noroo Paint, Republic of Korea) on a corona-treated PET film (thickness: 100 μm) and dried it at room temperature for 3 days. The coating specimen for the peel test was spray-coated onto the painted PET film using a commercial spray gun (LPH-80, ANEST IWATA, Japan) with a nozzle size of 1.2 mm and a pressure of 0.1 MPa (Scheme 2). This allowed us to measure the bonding force between the peelable coating and the paint layer.

The structure and morphology of the coating layer on the PET film were observed by FESEM (SUPRA 55VP, Carl Zeiss, Germany). The sample was dried in a vacuum oven at 60 °C for 12 h to remove moisture, and the cross section and surface were observed.

Determination of mechanical properties of the peelable coating film

Peel test

The 180° peel test was performed using a texture analyzer (TA-TX plus, Micro Stable Systems, UK) at a speed of 300 mm min^{-1}, temperature of 23 °C, and 50% relative humidity. The specimens coated on the substrates were prepared with a width of 25 mm after drying for 12 h at room temperature. In the time–load graph, the average load of the peak for a certain time interval is defined as the peel strength, and the average load of the depth, which is the height of the peak for the same interval, is calculated as drop-off. The applied force was recorded in N for three different runs, and the peel strength was calculated as the average force for a width of 25 mm (N/25 mm).

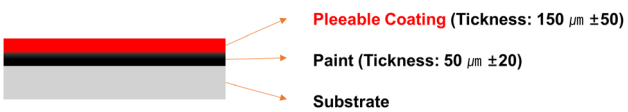

Scheme 2 Preparation of a peelable coating on a paint-coated substrate.

Tensile test

The tensile test was conducted using a universal testing machine (AllroundLine Z010, Zwick Co., Germany) according to ASTM D 638-14 at a cross-head speed of 300 mm min^{-1} at room temperature.

The specimens were prepared according to the dimensions of ASTM D638-14 Type IV specimens using a sample-cutting machine (WL1200 J, Withlab, Korea). Three specimens were measured to determine the tensile properties.

Viscoelastic properties

The temperature dependence of the dynamic storage modulus (G′) and the tan δ values of the adhesives were evaluated by dynamic mechanical analysis (DMA Q800, TA instruments, USA) in the film-tension mode in the temperature range of − 50 °C to 150 °C at a heating rate of 5 °C min^{-1}, strain rate of 0.1%, and frequency of 1 Hz. Flat specimens with approximately 11–13 mm length, 10 mm width, and 0.1 mm thickness were prepared.

Evaluation of hydrolysis of MPO

The hydrolysis experiments were performed at room temperature. In the case of coating films, rectangular specimens with a size of 10 × 10 × 0.015 mm (width × length × thickness) were prepared. The specimens were placed in 1 mL of a 4-EM aqueous solution (0.45 M) in a 1.5-mL vial, and MPO (6.2 mg, 0.025 mmol) was added to the suspension. A 20-μL aliquot was extracted from the reaction mixture and diluted with an aqueous solution of 4-EM (10 mL, 0.45 M). The hydrolysis reaction was observed by monitoring the formation of *p*-nitrophenoxide, which is the hydrolysis product of MPO, at λ_{max} = 407 nm by UV–visible spectroscopy (UV-2550, Shimadzu, Japan) [22–24].

Results and discussion

Characterization of waterborne SPUDs and UiO-66 catalyst

The reaction was monitored by performing FTIR spectroscopy of the reaction mixture during the synthesis. The FTIR spectra of the WPU prepolymer

and the synthesized SPUDs are shown in Fig. 1a–c. Three hours after the commencement of the synthesis, prepolymer I and TEA were added, followed by the addition of prepolymer II (after approximately 5 h) and APTES (Scheme 1a–c). In the final product formed after the addition of APTES to the prepolymer, the NCO group was capped with silicon. Thus, the peak at 2262 cm^{-1} disappeared. The intensity of the peak of the carbonyl group (C=O) and amino group (NH) of urethane slightly increased [25]. Figure 1c shows that the C = O group of both PU and esters gives rise to very strong peaks at 1714 cm^{-1}. The peaks for the OH stretching vibration were observed at 2948 cm^{-1}, while those for the bending vibration were observed at 1467 and 1116 cm^{-1}. Strong peaks for the stretching vibration appeared at 3332 cm^{-1} for NH_3, 1714 cm^{-1} for C = O, and 1240 cm^{-1} for CN, while the in-plane bending vibration peak of NH appeared at 1540 cm^{-1}, indicating the presence of polyuria groups (–NH–CO–NH–) [26, 27]. In addition, the symmetric stretching and bending vibrations of Si–O–Si networks were observed at 958 and 773 cm^{-1}, respectively [20, 25, 28].

As the k value (equilibrium constant) of the chemical reaction for the conversion of the ethoxy group of APTES to Si–OH after silane capping was not zero, the molecular weight and particle size of prepolymer II rather than those of the final product were measured. The measured M_w of prepolymer II was ~ 5500, and the particle size was ~ 150 nm.

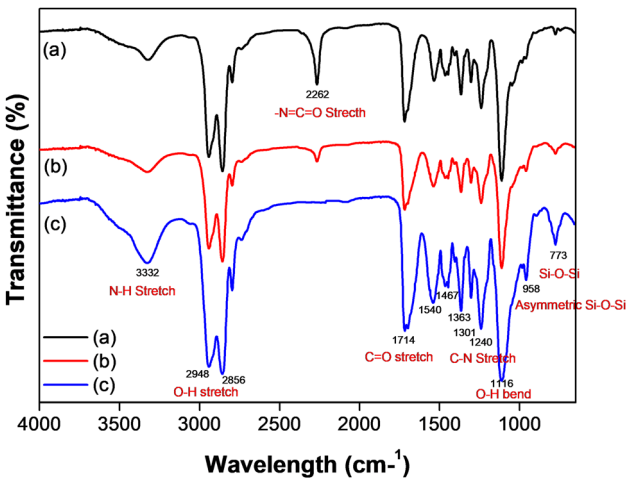

Figure 1 FTIR spectra of specimens in the synthesis of SPUD: (a) prepolymer I, (b) prepolymer II (chain extension), (c) final production (after capping).

The morphology and size of UiO-66 were investigated by FESEM (Fig. 2a). The PXRD profile of the synthesized UiO-66 is shown in Fig. 2b. The two most intensive peaks at 2θ = 7.3° and 8.5° can be indexed to the (111) and (200) crystal planes and are consistent with the previous reports [12, 29]. The BET specific surface area, total pore volume, and pore diameter were found to be 1075 m^2 g^{-1}, 0.37 cm^3 g^{-1}, and 1.39 nm, respectively.

Morphology of SPUD/UiO-66 peelable coating film

The cross sections of the SPUD/UiO-66 coating coated on painted substrates were observed to determine the distribution of the UiO-66 catalyst. The FESEM images are shown in Fig. 3. With increasing UiO-66 content, its dispersion in the polymer matrix improved. At a UiO-66 content of 60 wt%, the polymer binder content is low, and the cross section shows an empty space in the matrix after drying because of the aggregation of the UiO-66 catalyst. The surface porosity of the SPUD/PVB/UiO-66 coating film increased with increasing UiO-66 catalyst content (Fig. S1). This is because the content of the polymeric binder relatively decreased, which led to the polymer matrix acting as a bridge, resulting in the generation of many empty spaces.

Mechanical properties of the peelable coating film

Peel strength

In general, SPUDs show excellent adhesion to a variety of surfaces including PVC, glass, and steel substrates. This could be because of the reaction of the siloxane end group with the substrate surface. Fu et al. reported that the peel strength of a SPU film could be controlled by adjusting the molecular weight of polypropylene glycol during the synthesis of the SPU film for use as a pressure-sensitive adhesive [30]. For application in temporary protective coatings, the level of adhesion should be contained low enough to peel off from the substrate. Many temporary protective coatings are mainly composed of a polymer in an aqueous phase that can be easily removed from the substrate upon drying. In other cases, an additive is added to control the adhesion and viscosity [14, 31–35].

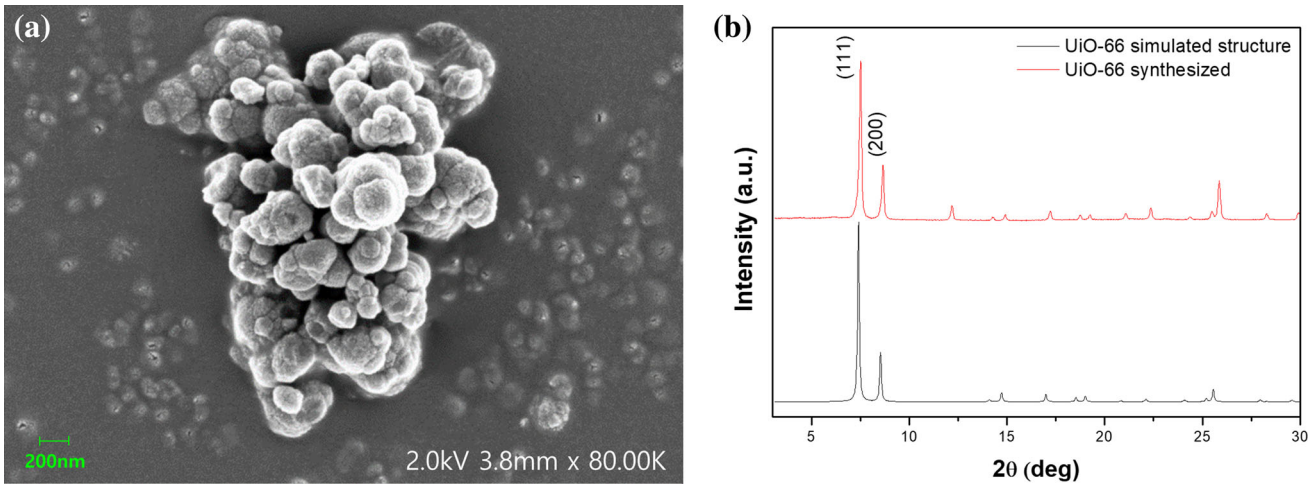

Figure 2 **a** FESEM images of synthesized UiO-66 and **b** PXRD profile of UiO-66 catalysts.

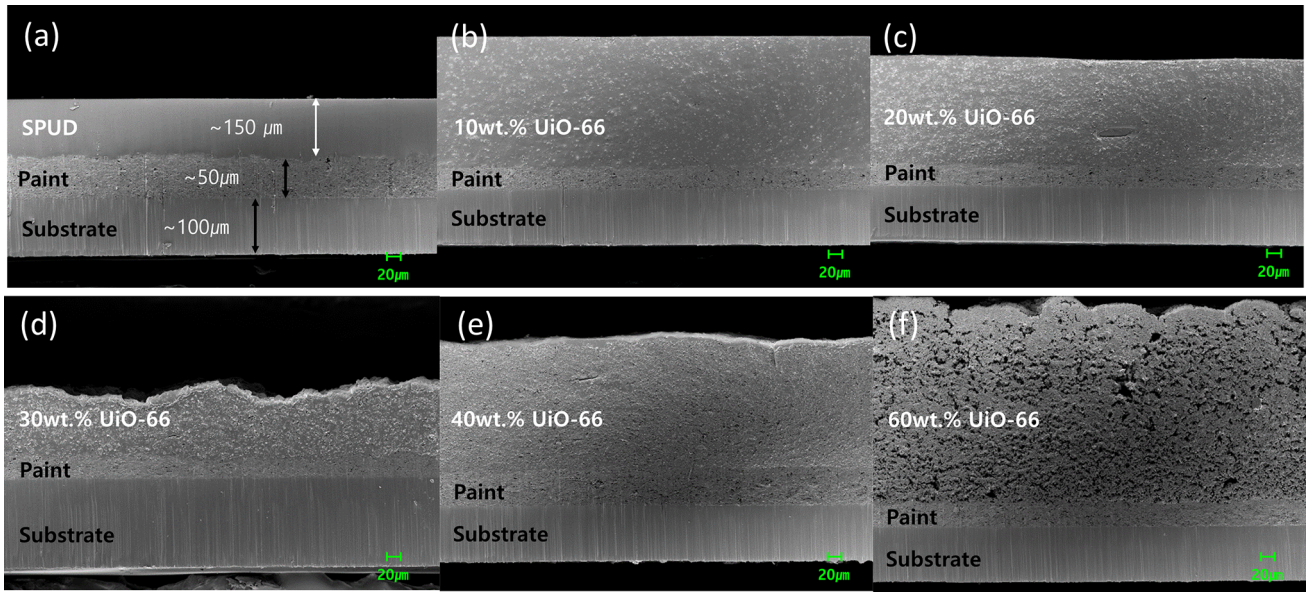

Figure 3 Cross-sectional FESEM images of SPUD/UiO-66 film, with **a** SPUD **b** 10 wt%, **c** 20 wt%, **d** 30 wt%, **e** 40 wt%, and **f** 60 wt% UiO-66, at ~ × 400 magnification.

First, the average peel strengths were measured for commercial peel-off products using various types of resins such as rubber, PVA, and PVB. All the films were coated onto painted substrates (Fig. 4a). In the case of a peelable coating, a certain film thickness was required for ease of peeling without stretching and tearing. The film could be easily removed from a glass substrate up to thickness of at least 500 μm [14]. The peel strength was measured according to the thickness of the rubber-based resin. When the thickness was more than or equal to 150 μm, the film could no longer be elongated (Fig. S2). The thickness of all the specimens was approximately 150 μm (standard deviation: ~ 50 μm). Figure 4a shows that the peel strength of rubber and the PVA resin is approximately 5 N/25 mm, whereas the average peel strength of the others is below 5 N/25 mm. Therefore, the peelable film had an average peel strength of ≤ 5 N/25 mm and could be easily peeled off.

According to Fig. 4b, the peel strength of the peelable coating film is affected by the content of the added catalyst. The average peeling force was affected by the catalyst content in the material. The peel strength of the SPUD/UiO-66 film slightly increased at 10 wt% of UiO-66 content and gradually decreased as the UiO-66 content increased. In particular, stick–

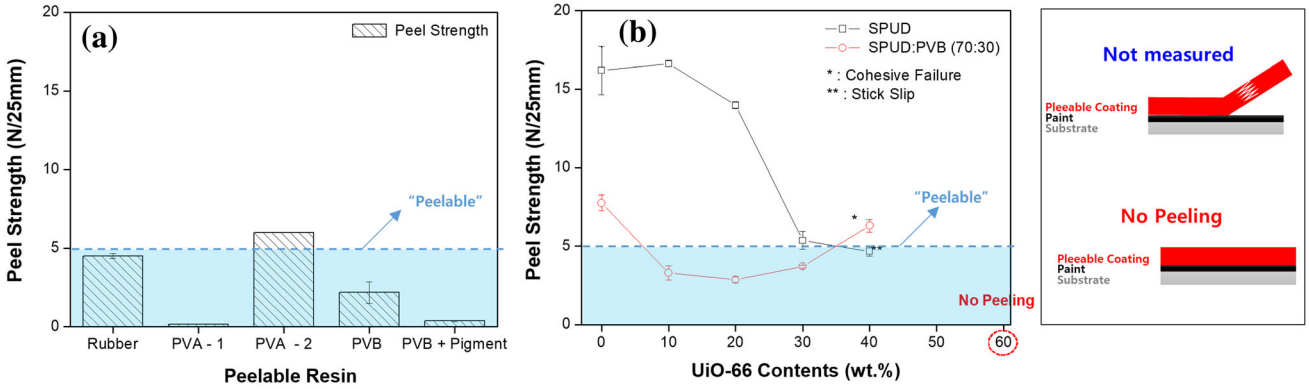

Figure 4 Peel average for **a** various peelable coatings and **b** SPUD/UiO-66 and SPUD/PVB/UiO-66 peelable coating.

slip occurred at 40 wt% of UiO-66 content (Fig. S3). At a UiO-66 content of 60 wt%, no peeling was observed. In the case of the SPUD/PVB/UiO-66 coating (SPUD: 70 wt%, PVB: 30 wt%), the average peel strength of the peelable coating film decreased up to 20 wt% of UiO-66 and then slightly increased to 30 wt% of UiO-66. At 40 wt% of UiO-66, the peel strength increased due to cohesive failure between the polymer coating film and the interface of the painted substrate. The polymeric coating film with 60 wt% UiO-66 could not be peeled off. Thus, the blend of SPUD and UiO-66 was unsuitable for peelable films, despite the good dispersion of the synthesized UiO-66 nanoparticles. However, the coating film containing the mixed SPUD and PVB binder was suitable for the peelable coating. In particular, the coating films with a UiO-66 content of up to 30 wt% could be easily removed.

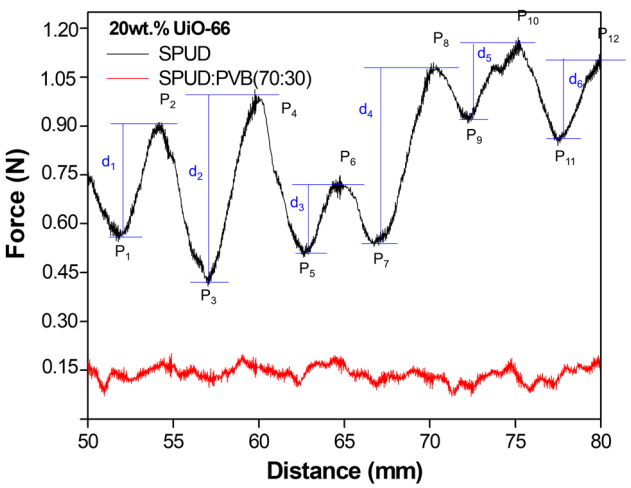

Figure 5 Time–load graph of the two different binder types.

Figure 5 shows the time–load graph of the two different binder types, SPUD and SPUD/PVB (70:30) with 20 wt% of UiO-66. The mean value of the force was determined as the peel strength by setting the interval for a certain time. We set the lowest and highest peaks for the same interval as P_{number}, respectively. $P_{n+1} - P_n$ was defined as the depth, and d_{number} was calculated. The average value [Eq. (4)] of the depths for a certain time interval was calculated as the drop-off value by expressing the peak height as the depth.

$$d_n = P_{n+1} - P_n \,(\text{Here}, P_n \text{ refers to the peak and trough values}) \tag{3}$$

$$\text{Drop - off}\ (N) = \frac{(d_1 + d_2 + d_3 + d_4 + d_5 + \cdots + d_n)}{n} / \text{n} \tag{4}$$

First, we calculated the drop-off value for a commercial peelable paint (Fig. 6a). Similar to the peel strength, the drop-off value differs depending on the resin type. The drop-off value was lower than 0.25 N overall. The drop-off values of rubber and PVA-1 are lower than 0.10 N, and those of PVA-2 and PVB are approximately 0.15 N. In the case of PVB + pigment, the drop-off value is approximately 0.07 N, similar to those of rubber and PVA-1. The drop-off value showed a trend similar to that of the average peel strength.

Figure 6b shows the drop-off values of the two binders according to the catalyst content. The drop-off value is 0.5 N or less for up to 30 wt% catalyst content regardless of the binder type. The drop-off value of the SPUD and PVB blend binder is similar to that of commercially available removable products

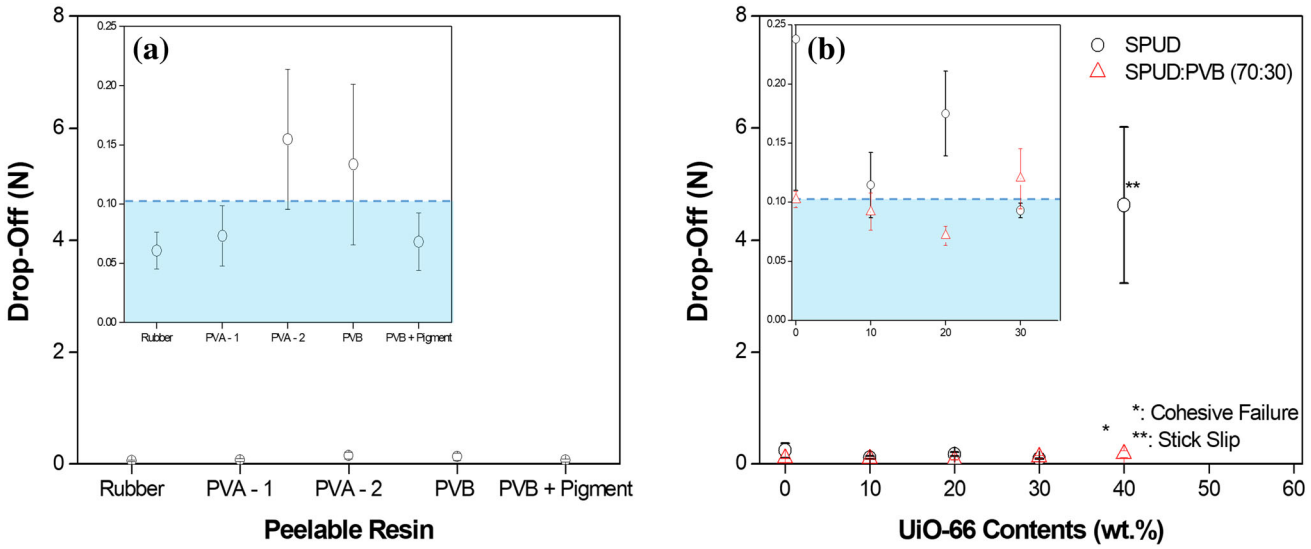

Figure 6 Drop-off with **a** various peelable coatings and **b** SPUD/UiO-66 and SPUD/PVB/UiO-66 peelable coating.

(approximately 0.10 N or less). However, for 40 wt% SPUD binder, the drop-off value is approximately 5 N. This is caused by the difference between the cohesive force between the coating films and the force acting at the interface between the substrate and the coating due to the stick–slip that occurred during the peel test. This is because a stick–slip occurred during peeling evaluation. Stick–slip is a phenomenon that occurs in the debonding process in which the coating film separates from the adherend. This is caused by the difference between the cohesive force of the coating film and the adhesion force between the coating film and the adherend. When the peelable coating is peeled from the adherend, a large contact pressure is applied. Tensile stress is concentrated at the bonding interface, so that compressive stress first occurs and then tensile stress is generated sequentially. As a result, stick–slip is a repetitive phenomenon of compressive stress and tensile stress at the bonded interface, explaining that the peelable coating is not easily peeled from the substrate. In the case of stick–slip, the peel strength is within the range of that required for easy peeling (approximately 5 N or less). However, the drop-off value indicates that the coating cannot be easily peeled off and thus is difficult to use as a peelable coating.

These results show that the relationship of the force between the substrate and the interface of the coating can be explained using the drop-off value, which is the depth of peak in the peeling test. The smaller the deviation of the depth of the peak, the stronger the cohesion between the coating films compared with the force acting between the coating film and the substrate. This implies that peeling is possible. As a result, it could be shown that not only the peel strength, but also the drop-off values determine the peelability of the coating.

Tensile properties

Fig. 7a shows that the strain–stress curve of the peelable coating film with the UiO-66 content in the SPUD binder. As the catalyst content increased, the Young's modulus increased, while the elongation decreased. At 60 wt% UiO-66, the film was too brittle, and the modulus and elongation at break rapidly decreased. In the case of the PVB and SPUD mixed binder, the Young's modulus increased sharply, and the elongation decreased with an increase in the catalyst content (Fig. 7b). At 60 wt% UiO-66 catalyst, the tensile strength of the polymer coating material could not be measured because it was too brittle. The results show that the physical properties of the polymer coating film improved when PVB was added.

Viscoelasticity

The viscoelastic behaviors of the films depending on the UiO-66 catalyst content of the polymeric SPU binders are shown in Fig. 8a, b. The incorporation of UiO-66 nanoparticles affected the storage modulus of

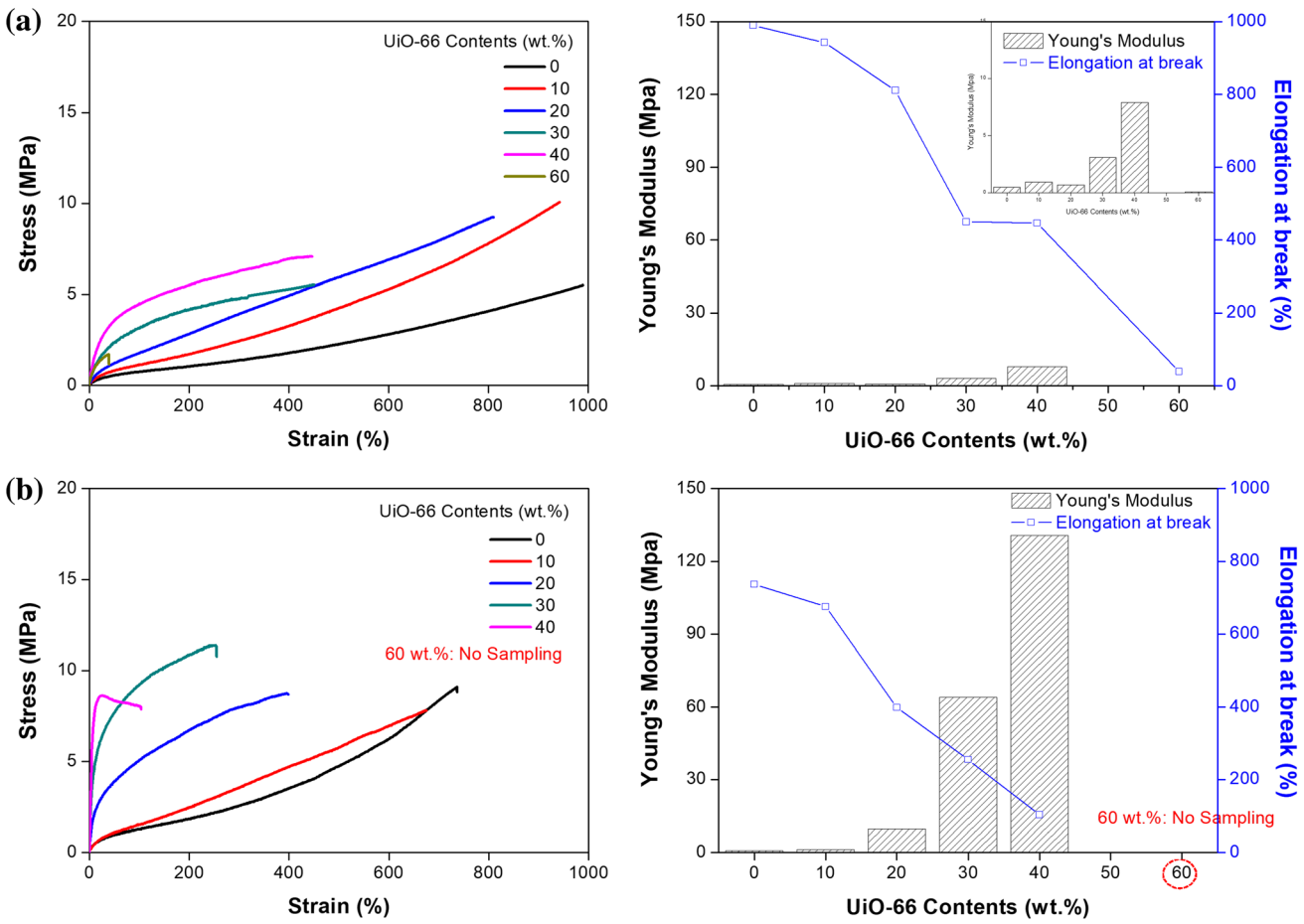

Figure 7 Strain–stress curve and tensile properties for **a** SPUD/UiO-66 film **b** SPUD/PVB/UiO-66 film.

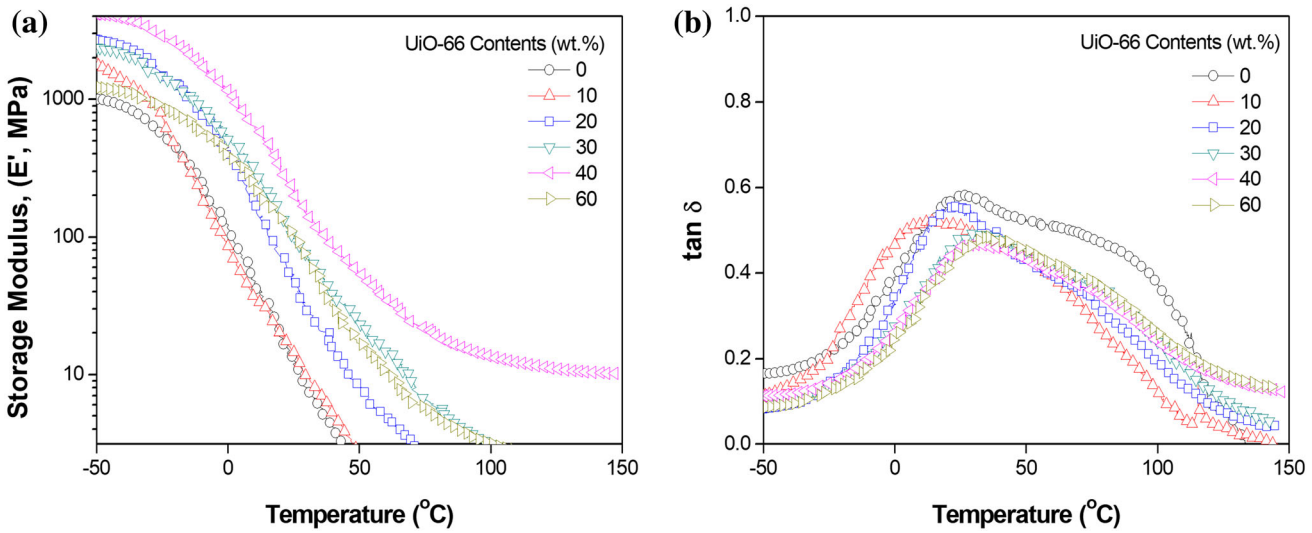

Figure 8 Graphs or plots of **a** storage modulus, E′ (log-scale) and **b** tan δ of the SPUD/UiO-66 peelable coating film (f = 0.1 Hz).

the peelable coating, but not the glass transition temperature (T_g). The storage modulus of the peelable coating film increased as the UiO-66 nanoparticle content increased up to 40 wt%. This was due to the "locking" effect between the nanoparticles and the primary and secondary PU

polymer chains with an increase in nanoparticle content of the polymer coating films. The polymer chains became much more rigid as the content of UiO-66 nanoparticles increased, as they immobilized the polymer chains, which were less likely to be relaxed due to binding with UiO-66 nanoparticles. According to Fig. 8b, the addition of nanoparticles to the SPUD hardly changed the T_g of the resulting peelable coating, which increased by ~ 10 °C. This implies that near the T_g, the mechanical response is dominated by the SPU matrix. The modulus of the polymer coating film containing 60 wt% UiO-66 dropped sharply. This indicates that when the nanoparticle content is higher than the content of polymer binder, only a small amount of polymer matrix is dominant in the mechanical reaction, and therefore, the mechanical reaction cannot properly proceed.

The measured T_g values of SPUD and PVB were approximately 28 °C and 82 °C, respectively. When SPUD and PVB were mixed, the T_g increased as the weight fraction of PVB increased (Fig. S6). The viscoelastic behavior of the SPUD and PVB mixed polymer binder with a PVB content of 30 wt% is shown in Fig. 9. In the glassy region ($T < T_g$), there is almost no difference in modulus; however, in the rubbery region ($T > T_g$), the modulus increased with increasing nanoparticle content. When the tan δ values were taken into account, one peak was observed for the neat polymer without the UiO-66 nanoparticles. When the UiO-66 nanoparticles were added, two peaks were observed. When the UiO-66 content increased, the height of the first peak decreased, and a second peak appeared, which was shifted to the right as compared with the T_g peak of the neat polymer. This suggests that the two peaks appeared due to an increase in the nanoparticle content of the blended polymeric binder, which increased the binding force between the nanoparticles and the binder compared with the force acting between the polymer and the binder. Thus, the interaction between the SPU matrix and nanoparticles occurred at a low UiO-66 content of 10 wt%, resulting in the first peak of tan δ. With an increase in the UiO-66 content, the interaction between PVB and the nanoparticles significantly increased, and the second peak shifted to the right [36].

Hydrolysis of MPO by the peelable coating film

The MPO hydrolysis reaction was monitored by the p-nitrophenoxide absorbance at 407 nm (Fig. 10). The conversion profile was calculated by the Beer–Lambert law for the absorbance of the p-nitrophenoxide peak [12, 21, 23, 24, 37]. Figure 11 shows the conversion rate of MPO as a function of the UiO-66 content in the SPUD/PVB/UiO-66 film. MPO decomposition experiments were carried out at time intervals of 0 min, 30 min, 60 min, 90 min, 2 h, 3 h, 6 h, 12 h, 1 day, 2 days, and 3 days. The decomposition performance increased with increasing reaction time. At 2 days, it reached the peak value of approximately 56–81%, and after that the conversion

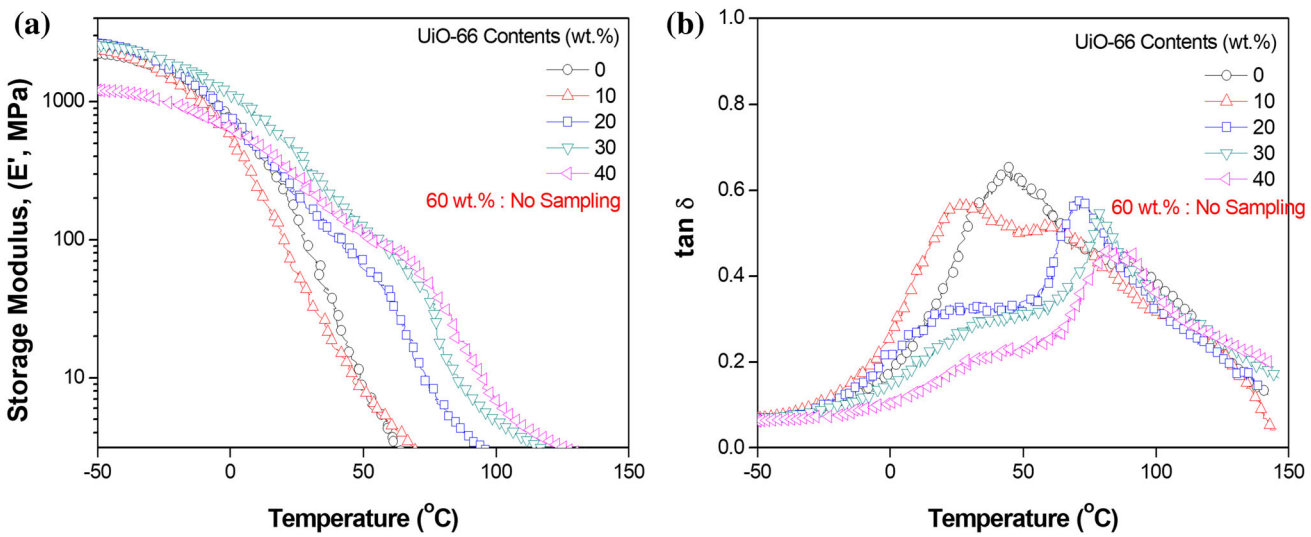

Figure 9 Graphs or plots of **a** storage modulus, E′ (log-scale) and **b** tan δ of the SPUD/PVB/UiO-66 peelable coating film (f = 0.1 Hz).

Figure 10 Hydrolysis of methyl paraoxon (MPO).

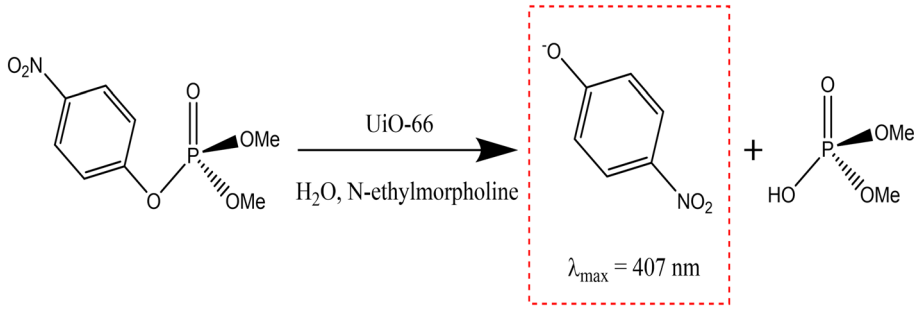

Hydrolysis of methyl para-oxon(MPO)

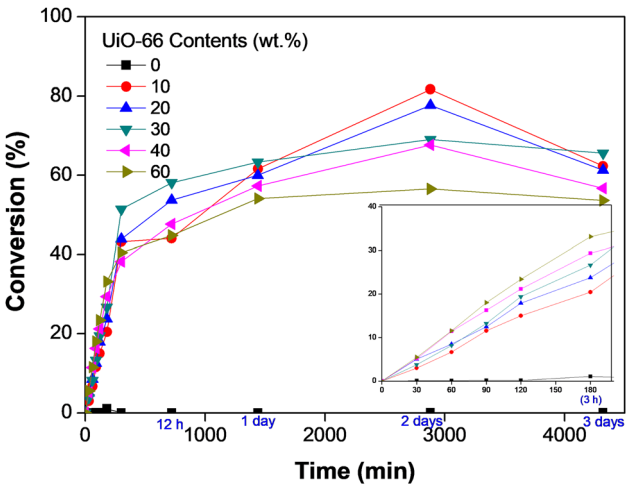

Figure 11 Conversion profiles for the decomposition of methyl paraoxon according to UiO-66 content in SPUD/PVB/UiO-66 film.

rate of MPO decreased or became constant. Such a decrease in MPO conversion with reaction time was reported to be due to the degraded activity of UiO-66 in the 4-EM aqueous solution under a high pH of 12 [38]. As shown in the FESEM micrographs, the SPUD/PVB/UiO-66 peelable coating film has a porous structure with many holes owing to the addition of PVB. The decomposition performance increased with an increase in the UiO-66 content for up to 1 d, and the MPO conversion was about 50% or more. Long et al. had measured the MPO conversion rate at 1 d by PU/UiO-66 film to be 36.0–63.2% [38]. This is comparable to the 50% or more MPO hydrolysis observed here and demonstrates that the added UiO-66 catalyst decomposed the nerve simulant. Particularly, at 2 d, the maximum decomposition performance was observed with a UiO-66 content of 10 wt%. Due to the porous structure of the film, the decomposition performance increased with increasing UiO-66 catalyst content, as the contact area between the catalyst and MPO increased. Over time, a high UiO-66 catalyst content is retained as a single large particle with no change in the contact area. However, in the case of a polymer film with a low UiO-66 catalyst content, it is expected that the binder swelled, and the contact area of the catalyst increased, thereby increasing the decomposition performance.

Conclusion

The peelability of SPUD/UiO-66 and SPUD/PVB/UiO-66 coating films used as peelable polymer coatings on paint-coated substrates was determined from the peel strength and drop-off value, and the relationship of the forces between the two coatings and the criteria for easy peeling were described. With an increase in the UiO-66 content in the SPUD/UiO-66 coating film, the modulus increased, while the elongation decreased. When PVB was added, the polymer coating film became brittle and its Young's modulus rapidly increased. The T_g of the polymer coating film produced by adding UiO-66 nanoparticles changed only slightly, indicating that the viscoelastic behavior is dominated by the SPUD matrix. Furthermore, the SPUD film with UiO-66 dispersed in the matrix could decompose the nerve agent simulant MPO. The decomposition performance of the SPUD/PVB/UiO-66 coating film increased with an increase in UiO-66 content for up to 1 day; however, afterwards that the decomposition value converged and the decomposition performance was approximately 50% or more. In conclusion, by using the synthesized SPU binder and UiO-66, a peelable coating with both good adhesion and decomposition performance could be successfully manufactured.

Acknowledgements

This work was supported by the National Research Council of Science and Technology (NST) grant by the Korean government (MSIP) (No. CMP-16-04-KITECH).

Author contributions

K-M Kim, H-J Kim, and S Shin designed the experiments. H-W Park, G-S Shim, and G Chae carried out the measurements. S-W Jang and J-H Lee analyzed the data. K-M Kim wrote the manuscript.

Electronic supplementary material: The online version of this article (https://doi.org/10.1007/s10853-019-04184-2) contains supplementary material, which is available to authorized users.

References

[1] Kreno LE, Leong K, Farha OK et al (2012) Metal–organic framework materials as chemical sensors. Chem Rev 112:1105–1125. https://doi.org/10.1021/cr200324t

[2] Lee J, Farha OK, Roberts J et al (2009) Metal–organic framework materials as catalysts. Chem Soc Rev 38:1450–1459. https://doi.org/10.1039/B807080F

[3] Liu J, Chen L, Cui H et al (2014) Applications of metal–organic frameworks in heterogeneous supramolecular catalysis. Chem Soc Rev 43:6011–6061. https://doi.org/10.1039/C4CS00094C

[4] Li J-R, Sculley J, Zhou H-C (2012) Metal–organic frameworks for separations. Chem Rev 112:869–932. https://doi.org/10.1021/cr200190s

[5] Mason JA, Veenstra M, Long JR (2014) Evaluating metal–organic frameworks for natural gas storage. Chem Sci 5:32–51. https://doi.org/10.1039/C3SC52633J

[6] Della Rocca J, Liu D, Lin W (2011) Nanoscale metal–organic frameworks for biomedical imaging and drug delivery. Acc Chem Res 44:957–968. https://doi.org/10.1021/ar200028a

[7] Moghadam PZ, Fairen-Jimenez D, Snurr RQ (2016) Efficient identification of hydrophobic MOFs: application in the capture of toxic industrial chemicals. J Mater Chem A 4:529–536. https://doi.org/10.1039/C5TA06472D

[8] Cavka JH, Jakobsen S, Olsbye U et al (2008) A new zirconium inorganic building brick forming metal organic frameworks with exceptional stability. J Am Chem Soc 130:13850–13851. https://doi.org/10.1021/ja8057953

[9] Schaate A, Roy P, Godt A et al (2011) Modulated synthesis of Zr-based metal–organic frameworks: from nano to single crystals. Chem Eur J 17:6643–6651. https://doi.org/10.1002/chem.201003211

[10] Liu X, Shen Z-Q, Xiong H-H et al (2015) Hierarchical porous materials based on nanoscale metal–organic frameworks dominated with permanent interparticle porosity. Microporous Mesoporous Mater 204:25–33. https://doi.org/10.1016/j.micromeso.2014.11.005

[11] Katz MJ, Brown ZJ, Colón YJ et al (2013) A facile synthesis of UiO-66, UiO-67 and their derivatives. Chem Commun 49:9449. https://doi.org/10.1039/c3cc46105j

[12] Cho KY, Seo JY, Kim H-J et al (2019) Facile control of defect site density and particle size of UiO-66 for enhanced hydrolysis rates: insights into feasibility of Zr(IV)-based metal–organic framework (MOF) catalysts. Appl Catal B Environ 245:635–647. https://doi.org/10.1016/j.apcatb.2019.01.033

[13] Natali I, Carretti E, Angelova L et al (2011) Structural and mechanical properties of "peelable" organoaqueous dispersions with partially hydrolyzed poly(vinyl acetate)-borate networks: applications to cleaning painted surfaces. Langmuir 27:13226–13235. https://doi.org/10.1021/la2015786

[14] Lewandowski K, Krepski LR, Mickus DE (2004) Dry-peelable temporary protective coatings from waterborne self-crosslinkable sulfourethane-silanol dispersions. J Appl Polym Sci 91:1443–1449. https://doi.org/10.1002/app.13316

[15] Shirai M, Bamba T, Hayashi K et al (2000) Sheet for protecting paint film

[16] Ozeki K, Wada T, Ito K et al (1982) Peelable film-forming urethane/isocyanate paints

[17] Rahman MM, Kim H-D, Lee W-K (2009) Properties of waterborne polyurethane adhesives: effect of chain extender and polyol content. J Adhes Sci Technol 23:177–193. https://doi.org/10.1163/156856108X344667

[18] Lei L, Zhong L, Lin X et al (2014) Synthesis and characterization of waterborne polyurethane dispersions with different chain extenders for potential application in waterborne ink. Chem Eng J 253:518–525. https://doi.org/10.1016/j.cej.2014.05.044

[19] Li S, Kong X, Feng S (2015) Preparation of uniform poly(urea-siloxane) microspheres through precipitation polymerization. RSC Adv 5:90313–90320. https://doi.org/10.1039/C5RA18140B

[20] Hou Z, Qu W, Kan C (2015) Synthesis and properties of triethoxysilane-terminated anionic polyurethane and its waterborne dispersions. J Polym Res 22:111. https://doi.org/10.1007/s10965-015-0757-8

[21] Kim K, Seo JY, Baek K-Y et al (2019) Metal–organic framework (UiO-66)-dispersed polyurethane composite

films for the decontamination of methyl paraoxon. Polym Int. https://doi.org/10.1002/pi.5856

[22] Mondloch JE, Katz MJ, Isley WC III et al (2015) Destruction of chemical warfare agents using metal–organic frameworks. Nat Mater 14:512–516. https://doi.org/10.1038/nmat4238

[23] Katz MJ, Mondloch JE, Totten RK et al (2014) Simple and compelling biomimetic metal–organic framework catalyst for the degradation of nerve agent simulants. Angew Chem 126:507–511. https://doi.org/10.1002/ange.201307520

[24] Katz MJ, Moon S-Y, Mondloch JE et al (2015) Exploiting parameter space in MOFs: a 20-fold enhancement of phosphate-ester hydrolysis with UiO-66-NH 2. Chem Sci 6:2286–2291. https://doi.org/10.1039/C4SC03613A

[25] Mirmohseni A, Akbari M, Najjar R, Hosseini M (2019) Self-healing waterborne polyurethane coating by pH-dependent triggered-release mechanism. J Appl Polym Sci 136:47082. https://doi.org/10.1002/app.47082

[26] Feng L, Iroh JO (2013) Novel polyimide-b-polyurea supramacromolecule with remarkable thermomechanical and dielectric properties. Eur Polym J 49:1811–1822. https://doi.org/10.1016/j.eurpolymj.2013.04.007

[27] Maya-Visuet E, Gao T, Soucek M, Castaneda H (2015) The effect of TiO_2 as a pigment in a polyurethane/polysiloxane hybrid coating/aluminum interface based on damage evolution. Prog Org Coat 83:36–46. https://doi.org/10.1016/j.porgcoat.2015.02.001

[28] Wu G, An J, Sun D et al (2014) Robust microcapsules with polyurea/silica hybrid shell for one-part self-healing anticorrosion coatings. J Mater Chem A 2:11614–11620. https://doi.org/10.1039/C4TA01312C

[29] Moghaddam ZS, Kaykhaii M, Khajeh M, Oveisi AR (2018) Synthesis of UiO-66-OH zirconium metal–organic framework and its application for selective extraction and trace determination of thorium in water samples by spectrophotometry. Spectrochim Acta A Mol Biomol Spectrosc 194:76–82. https://doi.org/10.1016/j.saa.2018.01.010

[30] Yuan Y, Zhang Y, Fu X et al (2016) Silane-terminated polyurethane applied to a moisture-curable pressure-sensitive adhesive using triethoxysilane. RSC Adv 6:83688–83696. https://doi.org/10.1039/C6RA19883J

[31] Blaine SJ, Wilson KK (1996) Protective solvent free liquid masking compounds and related method. US Patent 5,494,702, 27 Feb, 1996

[32] Muller H-P, Gruttmann H, Casselmann H, et al (1999) Cosolvent-free aqueous, anionic polyurethane dispersions and their use as peelable coatings. US Patent 5,965,195, 12 Oct, 1999

[33] Salamon PA 54) Temporary protective coatings for precision surfaces. 14

[34] Polymeric peel-off coating compositions and methods of use thereof. Google Patents US6124044A. https://patents.google.com/patent/US6124044A/en. Accessed 24 May 2019

[35] Adhesion performance of PSA–clay nano-composites by the in situ polymerization and mechanical blending. ScienceDirect. https://www.sciencedirect.com/science/article/pii/S0143749613001395. Accessed 2 July 2019

[36] Mahdi EM, Tan J-C (2016) Dynamic molecular interactions between polyurethane and ZIF-8 in a polymer-MOF nanocomposite: microstructural, thermo-mechanical and viscoelastic effects. Polymer 97:31–43. https://doi.org/10.1016/j.polymer.2016.05.012

[37] Li P, Klet RC, Moon S-Y et al (2015) Synthesis of nanocrystals of Zr-based metal–organic frameworks with csq-net: significant enhancement in the degradation of a nerve agent simulant. Chem Commun 51:10925–10928. https://doi.org/10.1039/C5CC03398E

[38] Long NH, Park H, Chae G et al (2019) Preparation of peelable coating films with a metal organic framework (UiO-66) and self-crosslinkable polyurethane for the decomposition of methyl paraoxon. Polymers 11:1298. https://doi.org/10.3390/polym11081298